BIOPRINTED PLURIPOTENT STEM CELL-DERIVED KIDNEY ORGANOIDS PROVIDE OPPORTUNITIES FOR HIGH CONTENT SCREENING

William Higgins[1], Alison Chambon[1], Kristina Bishard[1], Anke Hartung[1], Derek Arndt[1], Jamie Brugnano[1], Pei Xuan Er[1], Kynan T. Lawlor[1], Jessica M. Vanslambrouck[2], Sean B. Wilson[2], Alexander N. Combes[2,3], Sara E. Howden[2], Ker Sin Tan[2], Santhosh V. Kumar[2], Lorna J. Hale[2], Stephen Pentoney[1], Sharon C. Presnell[1], Benjamin R. Shepherd[1], Alice E. Chen[1] and Melissa H. Little[2,3]

1. Organovo Inc, San Diego, CA, USA 2. Murdoch Children's Research Institute, VIC, Australia 3. The University of Melbourne, VIC, Australia

Submission ID #: 671132

Poster #: T-4013

ABSTRACT

Recent progress in the directed differentiation of human pluripotent stem cells to kidney organoids advances the prospect of drug screening, disease modeling, and even restoration of renal function using patient-derived stem cell lines. Here, we demonstrate the successful adaptation of our directed differentiation protocol to the NovoGen Bioprinter® MMX technology to achieve automated, rapid fabrication of self-organizing kidney organoids. Bioprinted organoids were found to be equivalent to those previously reported via manual generation at the level of morphology, component cell types, and expression profiles. Bioprinted kidney organoids treated with doxorubicin exhibited concentration-dependent toxicity, characterized by the loss of podocyte-specific markers. High-throughput toxicity screening was achieved by treating organoids bioprinted in 96-well plates with a classic nephrotoxic compound. Collectively, these results suggest that bioprinted kidney organoids are functionally equivalent to those prepared manually and thus are likely to be useful for a multitude of applications.

METHODS

All iPSC culture and differentiation procedures were performed following published methodologies (Takasato et. al 2015, 2016) with slight modifications as noted in Higgins et. al 2018.

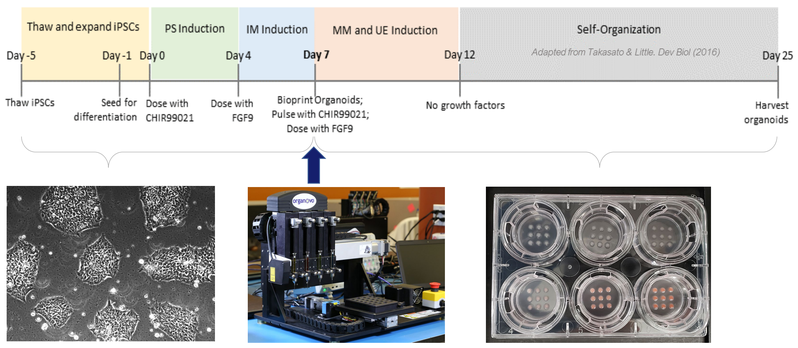

Figure 1: Methods overview for the inclusion of NovoGen Bioprinter® MMX technology in the generation of kidney organoids. Schematic outline of 2D differentiation, generation of 3D organoids by bioprinting, and culture of kidney organoids through maturation at D25 (D7+18).

RESULTS

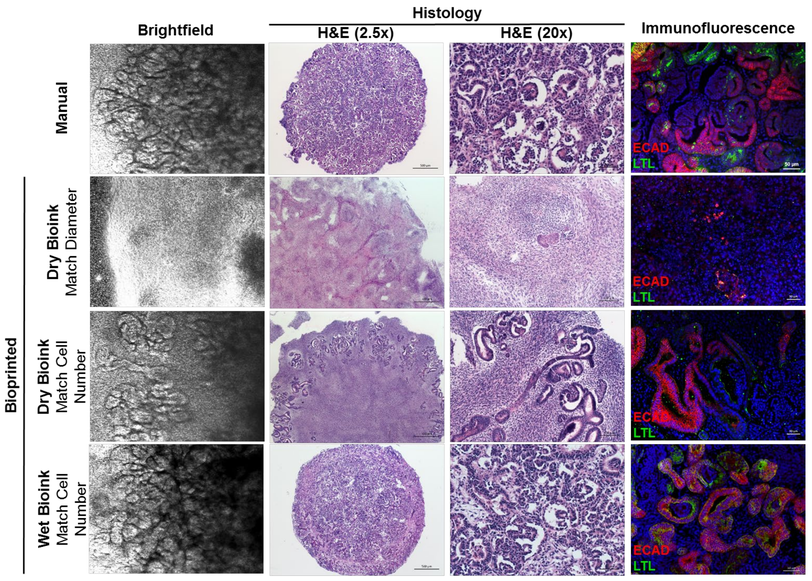

Figure 2: Optimization of bioprinting methodology for the generation of kidney organoids. Brightfield, histological, and immunofluorescence comparisons of kidney organoids generated manually (5 x 10^5 cells per organoid) with bioprinted organoids using dry cell paste (bioink) controlled for organoid diameter, dry bioink controlled for cell number, and wet bioink controlled for cell number. Immunofluorescent characterization of Day 25 organoids showing the presence/absence of tubular epithelium (E-CADHERIN, red) and proximal tubules (LTL, green).

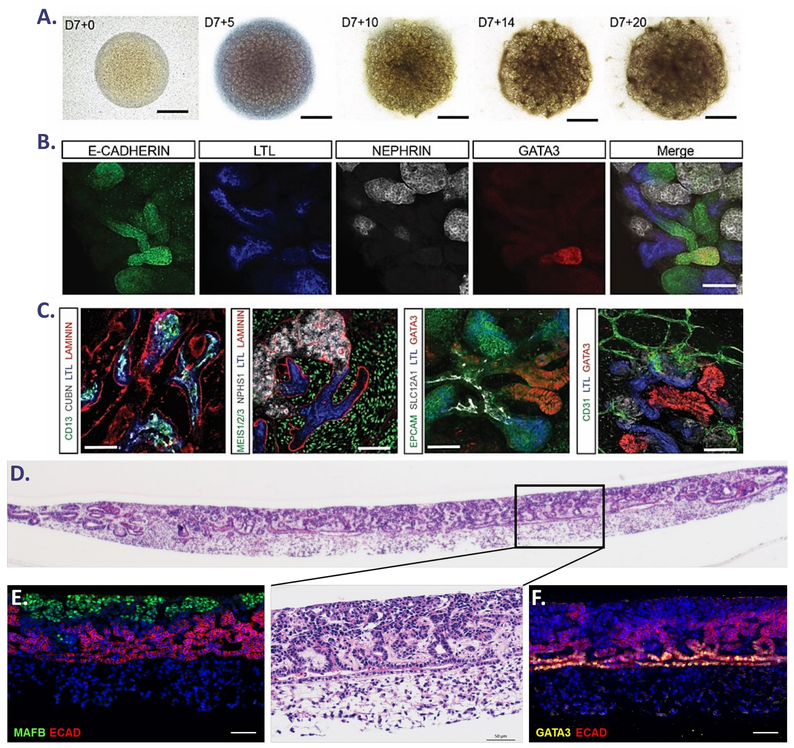

Figure 3: Characterization of kidney organoids bioprinted using control and reporter iPSC lines. **[A]** Brightfield images of bioprinted organoids across time showing evidence of increasing tubular complexity. Scale bar represents 800 µm. **[B]** Immunofluorescence of a Day 25 bioprinted organoid showing the presence of nephron epithelium (E-CADHERIN, green), proximal tubules (LTL, blue), collecting duct (GATA3, red) and podocytes (NEPHRIN, grey). Scale bar represents 100 µm. **[C]** Immunofluorescence of Day 25 bioprinted organoids stained for the proximal tubule markers CD13, LTL and CUBN, podocyte marker NPHS1, distal tubule epithelial markers EPCAM and SLC12A1, collecting duct markers EPCAM and GATA3, the presence of a LAMININ-positive basement membrane along the nephrons, a surrounding MEIS1/2/3-positive stroma and CD31-positive endothelium. Scale bar represents 50µm. **[D]** Histological cross-section of bioprinted organoids showed a high level of tissue organization. **[E]** MAFB$^+$ podocytes reside in close proximity to ECAD$^+$ tubular regions. **[F]** A contiguous putative collecting duct (GATA3$^+$/ECAD$^+$) network spans horizontally throughout organoids with nephrons connected to and contiguous with this epithelium. Scale bar (E-F) represents 50 µm.

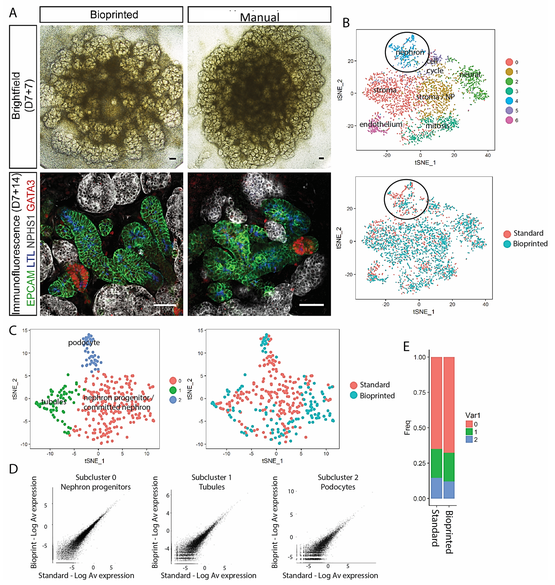

Figure 4: Single cell transcriptional profiling shows equivalence between standard and bioprinted kidney organoids. **[A]** Brightfield and immunofluorescent characterization of maturing kidney organoids generated manually and with bioprinting. Day 14 (D7+7) brightfield images show complex, maturing organoid structures with congruence between production methods. Day 21 (D7+14) organoids confirm key nephron structures across both methodologies with presence of tubule epithelia (EPCAM, green), proximal tubule cells (LTL, blue), podocytes (NPHS1, grey), and collecting duct (GATA3, red). **[B]** tSNE overlay of 3885 cells isolated from manual or bioprinted kidney organoids. Unsupervised clustering with Seurat identified 7 distinct cell clusters and direct comparison with standard organoids, identified as indicated using GO analysis and comparison to available human fetal kidney data (Lindstrom et al., 2018). A view of the same tSNE plot indicating whether individual cells were derived from the manual (blue) or bioprinted (pink) organoids. **[C]** Reanalysis of the nephron cluster (cluster 4) reveals the presence of three subclusters, identifiable as committed progenitor / renal vesicle (subcluster 0), early tubule (subcluster 1) and podocyte (subcluster 2). tSNE plot identifying nephron cluster cells based upon their origin in either manual (blue) or bioprinted (pink) organoids. **[D]** A comparison of average gene expression values (each point is a gene) within each nephron subcluster between manual and bioprinted organoids shows tight transcriptional conformity. **[E]** Relative proportion of cells present in each subcluster for manual and bioprinted organoids.

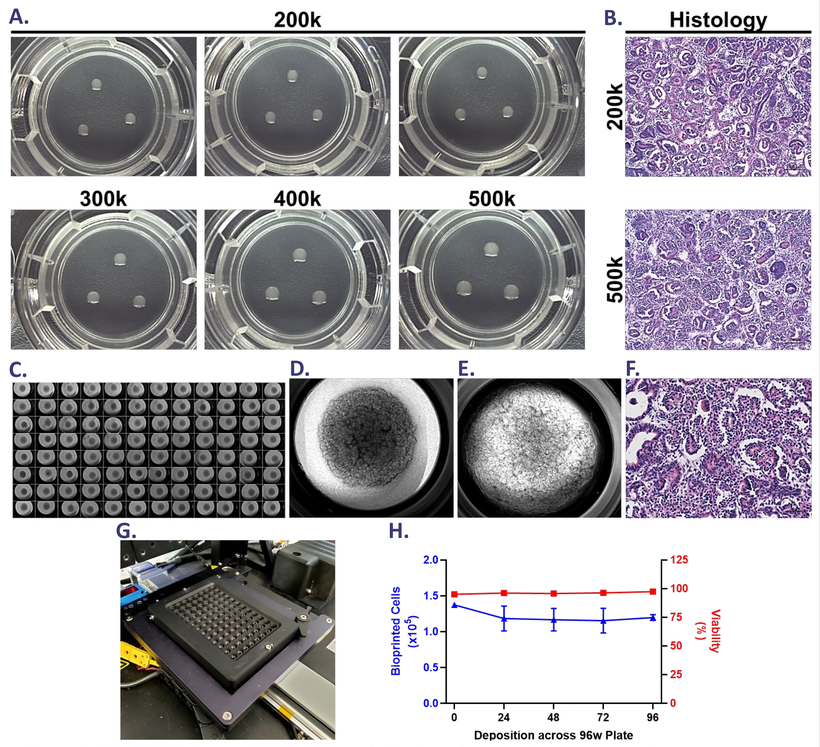

Figure 5: Bioprinted kidney organoid differentiation is equivalent with reduced starting cell number. **[A]** Images show three kidney organoids bioprinted within a single Transwell™ permeable support at 2x10^5, 3x10^5, 5x10^5,and 5x10^5 cells per organoid. **[B]** H&E stains of sectioned organoids bioprinted at 2x10^5 and 5x10^5 cells/organoid. **[C]** Composite panel of 1x10^5 cells/organoid bioprinted into each well of a 96-well Transwell™ permeable support system. **[D]** Representative maturing kidney organoid printed on 96-well Transwell™ permeable support at Day 15 (Day 7+8) and **[E]** Day 25 (Day 7+18). **[F]** H&E stains of a sectioned Day 25 (Day 7+18) mature organoid bioprinted on a 96-well Transwell™ permeable support. **[G]** Prototype 96-well anti-rotational plate to facilitate printing on Transwell permeable supports. **[H]** Bioink concentration and viability showed stability throughout the full 96-well bioprinting process.

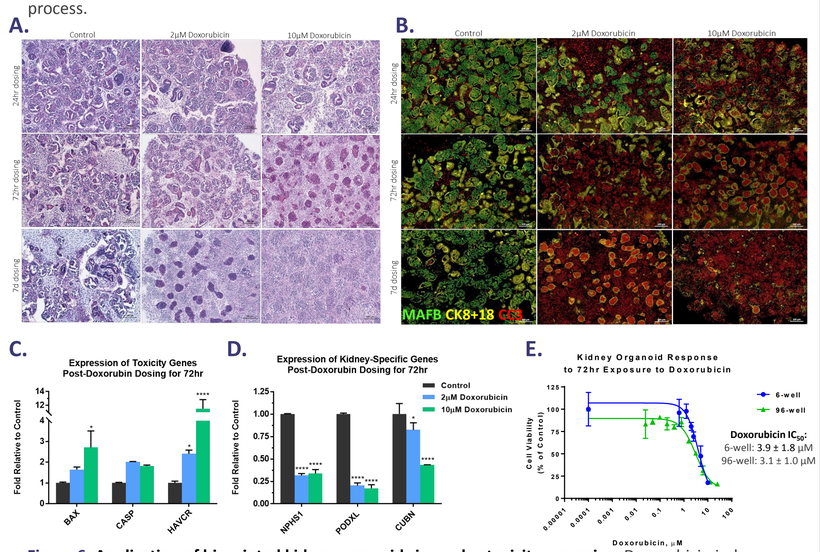

Figure 6: Application of bioprinted kidney organoids in nephrotoxicity screening. Doxorubicin induces a compartment-specific toxic response to glomerular cell types. **[A]** H&E staining of kidney organoids show a time- and dose-dependent toxic response to doxorubicin. **[B]** Immunofluorescent staining of sectioned organoids after doxorubicin exposure for podocytes (MAFB, green); tubular epithelium (CK8/18, yellow); Apoptosis (Cleaved Caspase 3, red). Kidney organoids exhibit a rapid loss of glomerular marker MAFB and increase of CC3 in response to doxorubicin. **[C]** Doxorubicin treatment leads to up-regulation of apoptosis and kidney injury genes (BAX, CASP3, HAVCR). **[D]** Preferential down-regulation of nephron markers (NPHS1, PDXL) compared to the proximal tubule marker (CUBN) upon doxorubicin treatment. Significant differences in gene expression calculated relative to control organoid expression (n=2 to 3 organoids per treatment group), and assessed by Two-Way ANOVA with Dunnett's Multiple Comparisons, *p<.05, ****p<.0001. **[E]** Viability of cells within kidney organoids bioprinted in either 6-well (n=3-6 per doxorubicin concentration) or 96-well (n=1-3 organoids per doxorubicin concentration) format in response to 72-hr treatment with doxorubicin.

CONCLUSION

3D Bioprinting enables automated and scaled fabrication of human iPSC-derived kidney organoids equivalent to those generated manually at the level of cellular complexity, identity, and gene expression. In addition, inclusion of the bioprinter increased speed and reproducibility facilitating larger production runs without comprising organoid quality. This work suggests significant utility for drug testing and modeling human development and disease *in vitro*, and provides translational promise for the combined use of iPSC and tissue engineering technologies for functional restoration in patients with renal disease.

REFERENCES

- Higgins JW, Chambon A, Bishard K, Hartung A, Arndt D, Brugnano J, Xuan Er P, Lawlor KT, Vanslambrouck JM, Wilson S et al (2018) Bioprinted pluripotent stem cell-derived kidney organoids provide opportunities for high content screening. bioRxiv https://doi.org/10.1101/505396505396 [PREPRINT]
- Lindström, N. O. et al. Conserved and divergent features of mesenchymal progenitor cell types within the cortical nephrogenic niche of the human and mouse kidney. J. Am. Soc. Nephrol. 29, 806–824 (2018).
- Takasato, M., Pei, X.E., Chiu, H.S., Maier, B., Baillie, G.J., Ferguson, C., Parton, R.G., Wolvetang, E.J., Roost, M.S., de Sousa Lopes, S.M.C. and Little, M.H., 2015. Kidney organoids from human iPS cells contain multiple lineages and model human nephrogenesis. *Nature*, *526*(7574), p.564.
- Takasato, M. and Little, M.H., 2016. A strategy for generating kidney organoids: recapitulating the development in human pluripotent stem cells. Developmental biology, 420(2), pp.210-220.